ARMY RESEARCH LABORATORY

Numerical Simulations of Supersonic Flow Over an Elliptic Section Projectile With Jet Interaction

Jubaraj Sahu

ARL-TR-2976

MAY 2003

NOTICES

Disclaimers

The findings in this report are not to be construed as an official Department of the Army position unless so designated by other authorized documents.

Citation of manufacturers' or trade names does not constitute an official endorsement or approval of the use thereof.

DESTRUCTION NOTICE—Destroy this report when it is no longer needed. Do not return it to the originator.

Army Research Laboratory
Aberdeen Proving Ground, MD 21005-5066

ARL-TR-2976 May 2003

Numerical Simulations of Supersonic Flow Over an Elliptic Section Projectile With Jet Interaction

Jubaraj Sahu
Weapons & Materials Research Directorate

INTENTIONALLY LEFT BLANK

REPORT DOCUMENTATION PAGE

Form Approved
OMB No. 0704-0188

1. REPORT DATE *(DD-MM-YYYY)*	2. REPORT DATE	3. DATES COVERED (From - To)
May 2003	Final	

4. TITLE AND SUBTITLE

Numerical Simulations of Supersonic Flow Over an Elliptic Section Projectile With Jet Interaction

5a. CONTRACT NUMBER

5b. GRANT NUMBER

5c. PROGRAM ELEMENT NUMBER

6. AUTHOR(S)

Sahu, J. (ARL)

5d. PROJECT NUMBER
1L1612618AH80

5e. TASK NUMBER

5f. WORK UNIT NUMBER

7. PERFORMING ORGANIZATION NAME(S) AND ADDRESS(ES)

U.S. Army Research Laboratory
Weapons & Materials Research Directorate
Aberdeen Proving Ground, MD 21005-5066

8. PERFORMING ORGANIZATION REPORT NUMBER
ARL-TR-2976

9. SPONSORING/MONITORING AGENCY NAME(S) AND ADDRESS(ES)

10. SPONSOR/MONITOR'S ACRONYM(S)

11. SPONSOR/MONITOR'S REPORT NUMBER(S)

12. DISTRIBUTION/AVAILABILITY STATEMENT

Approved for public release; distribution is unlimited.

13. SUPPLEMENTARY NOTES

14. ABSTRACT

Computational fluid dynamics (CFD) approaches were used to compute the supersonic flow fields and aerodynamic forces and moments on an elliptic projectile with jet interaction. Steady state numerical results have been obtained for the jet interaction problem at a supersonic Mach number, Mach = 4.0, and several angles of attack from 0° to 12° via Navier-Stokes computational techniques. The jet modeled in this problem is a supersonic helium jet exhausted into the free stream flow at a high pressure. Computed CFD results show the qualitative features and strong flow interaction between the jet and the free-stream flow. In general, very good agreement of the computed aerodynamic coefficients with the experimental data was achieved for all angles of attack investigated for the "jet-on" conditions. The results show the predictive capabilities of CFD techniques for supersonic flow over elliptic projectiles with jet interaction.

15. SUBJECT TERMS

chimera computational fluid dynamics projectile and missile aerodynamics structured grids unstructured grids

16. SECURITY CLASSIFICATION OF			17. LIMITATION OF ABSTRACT	18. NUMBER OF PAGES	19a. NAME OF RESPONSIBLE PERSON
a. REPORT	b. ABSTRACT	c. THIS PAGE			Jubaraj Sahu
Unclassified	Unclassified	Unclassified	UL	27	19b. TELEPHONE NUMBER *(Include area code)* 410-278-3707

INTENTIONALLY LEFT BLANK

Contents

List of Figures v

Acknowledgments vii

1. Introduction 1

2. Solution Techniques 2

2.1 CFD++ Flow Solver 2

2.2 Chimera Composite Grid Scheme 4

3. Computational Grids 4

4. Results 9

5. Concluding Remarks 16

6. References 17

List of Figures

Figure 1. H3P78 projectile 5

Figure 2. Full grid for viscous computations, jet on 5

Figure 3. Expanded view of the grid in the base region, jet on 6

Figure 4. Circumferential cross section of the grid at the base 6

Figure 5. Expanded view of the jet grids projected onto the projectile surface 7

Figure 6. Expanded view of the grid near the jet with nozzle modeling: (a) top view, (b) side view 8

Figure 7. H3P78 projectile showing the jet locations 9

Figure 8. Computed helium concentration contours near the base region, angle of attack, α = (a) 0°, (b) 4°, (c) 8°, and (d) 12°, M = 4.0 10

Figure 9. Computed surface pressure contours, jet on, angle of attack, α = (a) 0°, (b) 4°, (c) 8°, and (d) 12°, M = 4.0 12

Figure 10. Experimental surface pressure measurement points, M = 4.0 13

Figure 11. Surface pressure comparison along the centerline of symmetry, M = 4.0 13

Figure 12. Surface pressure comparison along the centerline of jet, M = 4.0 14

Figure 13. Normal force coefficient, M = 4.0 14

Figure 14. Pitching moment coefficient, M = 4.0 15

Figure 15. Application factor, M = 4.0 15

INTENTIONALLY LEFT BLANK

Acknowledgments

The authors wish to thank D. M. Orchard, Qinetiq, United Kingdom (UK); E. Fournier, Defence Research Establishment, Valcartier, Canada; and J. A. Edwards, Defence Evaluation and Research Agency, UK, for all their help in providing the experimental data to validate the computed results. Special thanks to D. M. Orchard for all the discussions and assistance in the analysis of the data. The authors wish to thank S. R. Chakravarthy and his colleagues of Metacomp Technologies for all their help with the application of CFD++ code to this problem. The scientific visualization work of R. Angelini of the U.S. Army Research Laboratory (ARL) and the computational support of ARL's Major Shared Resource Center are greatly appreciated.

INTENTIONALLY LEFT BLANK

1. Introduction

The advancement of computational fluid dynamics (CFD) has had a major impact on projectile design and development **[1 through 4]**. Improved computer technology and state-of-the-art numerical procedures enable solutions to complex, three-dimensional (3-D) problems associated with projectile and missile aerodynamics. In general, these techniques produce accurate and reliable numerical results for projectiles and missiles at small angles of attack. Modern projectiles and missiles are expected to experience moderate to large angles of attack during flight. Of particular interest is the accurate determination of supersonic and hypersonic flow over elliptic projectiles at moderate angles of attack. The flow field for such projectiles with non-axisymmetric cross sections is complex, especially in the presence of jets used to maneuver these projectiles. The work presented in this report was initiated as part of The Technical Cooperation Program (TTCP) effort with participants from Canada, the United Kingdom, and the United States and was aimed at assessing the capabilities of Euler and Navier-Stokes solvers currently available to research scientists for supersonic flow over elliptic projectiles for both "jet-off" and "jet-on" conditions **[5,6]**. The TTCP research effort has also focused on the wind tunnel testing as well as free flight testing of these projectiles. Different aspects of computational techniques such as grid generation, algorithms, turbulence modeling, and flow field visualization have been addressed by the group.

Earlier, inviscid solutions were obtained for H-series projectiles by the zonal Euler solver (ZEUS) graphical user interface (GUI) code **[7]**. Since H-series projectiles are not axisymmetrical, the projectile surface was generated by an auxiliary program and written as a set of discrete points to a file. The projectile surface was read into ZEUS GUI with the user-defined surface option. Pitch plane symmetry was used for most computations. Computations of the H3 projectile and its variations (with and without flares and strakes) were performed with the Euler ZEUS code at M = 8.2 and several angles of attack between 0° and 15°. A comparison was made of stabilization by strakes and flares for a different H-series projectile. The computations indicated that although the flares gave increased drag, they were still substantially more effective in providing stability than strakes alone. Recently, CFD techniques have been applied for the numerical prediction of supersonic flow over the elliptic H3P78 projectile **[8]**.

Calculations for the H3P78 projectile were performed with the ZEUS Euler code and two Navier-Stokes flow solvers: the zonal Navier-Stokes flow (ZNSFLOW) **[9]** solver and CFD++ **[10, 11]**, at several supersonic Mach numbers between 2.5 and 4.0 and several angles of attack from 0° to 12° for the jet-off conditions. Computed aerodynamic coefficients were found to be in very good agreement with the experimental data in all cases. The present research focuses on the application of advanced CFD techniques for accurate numerical prediction of supersonic flow over the elliptic H3P78 projectile with jet interaction. Numerical computations for the H3P78

projectile have been performed for the jet-on conditions by CFD++ code to study the interaction of a helium jet with a free stream, M = 4.0, flow at several angles of attack.

A description of the computational techniques is presented, followed by a description of the applications of these techniques to the H3P78 projectile. Results for this configuration are presented at Mach 4 and several angles of attack (0° to 12°) at various supersonic speeds. Computed data have been compared with experimental data provided by the Defence Evaluation and Research Agency (DERA) **[5]**, United Kingdom (UK), and obtained at Defence Research Establishment, Valcartier, Canada **[12].**

2. Solution Techniques

2.1 CFD++ Flow Solver

The basic numerical framework in which the proposed scheme is implemented is termed the unified grid, unified physics, and unified computing framework. These have been implemented in a software suite called CFD++ **[10, 11],** and the user is referred to these references for details of the basic numerical framework. Here, only a brief synopsis of this framework and methodology is given.

The 3-D, time-dependent Reynolds-averaged Navier-Stokes (RANS) equations are solved by the following finite volume method:

$$\frac{\partial}{\partial t}\int_V \mathbf{W} dV + \oint [\mathbf{F} - \mathbf{G}] \cdot dA = \int_V \mathbf{H} dV \qquad (1)$$

in which **W** is the vector of conservative variables, **F** and **G** are the inviscid and viscous flux vectors, respectively, **H** is the vector of source terms, V is the cell volume, and A is the surface area of the cell face.

The numerical framework of CFD++ is based on the following general elements:

1. unsteady compressible and incompressible Navier-Stokes equations with turbulence modeling (unified physics);

2. unification of Cartesian, structured curvilinear, and unstructured grids, including hybrids (unified grid);

3. unification of treatment of various cell shapes, including hexahedral, tetrahedral, and triangular prism cells (3-D), quadrilateral and triangular cells (two-dimensional) and linear elements (one-dimensional) (unified grid);

4. treatment of multi-block patched aligned (nodally connected), patched nonaligned and overset grids (unified grid);

5. total variation diminishing discretization based on a new multi-dimensional interpolation framework;

6. Riemann solvers to provide proper signal propagation physics, including versions for preconditioned forms of the governing equations;

7. consistent and accurate discretization of viscous terms via the same multi-dimensional polynomial framework;

8. point-wise turbulence models that do not require knowledge of distance to walls;

9. versatile boundary condition implementation which includes a rich variety of integrated boundary condition types for the various sets of equations; and

10. implementation on massively parallel computers based on the distributed memory message-passing model that uses native message-passing libraries or message-passing interfaces, parallel virtual machine, etc. (unified computing).

The code has brought together several ideas about convergence acceleration to yield a fast methodology for all flow regimes. The approach can be labeled as a "preconditioned implicit relaxation" scheme. It combines three basic ideas: implicit local time stepping, relaxation, and preconditioning. Preconditioning the equations ideally equalizes the eigenvalues of the inviscid flux Jacobians and removes the stiffness arising from large discrepancies between the flow and sound velocities at low speeds. The use of an implicit scheme circumvents the stringent stability limits suffered by their explicit counterparts, and successive relaxation allows cells to be revised as information becomes available and thus aids convergence.

The code has recently added the ability to deal with multi-block meshes with various types of inter-block connectivities. Multi-dimensional interpolation more accurately represents local behavior of flow-dependent variables. While the formal order of accuracy need not be any higher, this approach leads to practically higher accuracy on relatively coarse meshes. The multi-dimensional interpolation framework helps us deal easily with inter-block connectivities as well. Second order discretization was used for the flow variables and the turbulent viscosity equation. The turbulence closure has been based on topology-parameter-free formulations. These models are ideally suited to unstructured bookkeeping and massively parallel processing because of their independence from constraints related to the placement of boundaries and/or zonal interfaces. Recent contributions to these models include the following:

a. improved behavior of the dissipation rate transport equation by explicit sensitization to non-equilibrium flow regions, and

b. enhanced near-wall characteristics and elimination of *ad hoc* formulations through the introduction of time scale realization.

2.2 Chimera Composite Grid Scheme

The chimera overset grid technique greatly adds to the number of applications to which the CFD++ solver can be applied. The Chimera overset grid technique, which is ideally suited to complex configurations and multi-body problems **[1 through 4, 13, 14, 15]**, involves the generation of independent grids about each body or component and then oversetting them onto a base grid to form the complete model. An advantage of the overset grid technique is that it allows computational grids to be obtained for each body component separately and thus makes the grid generation process easier. Because each component grid is generated independently, portions of one grid may lie within a solid boundary contained within another grid. Such points lie outside the computational domain and are excluded from the solution process. Equation 1 has been modified to accommodate chimera overset grids that allow the possibility of having arbitrary holes in the grid. The set of grid points that forms the border between the hole points and the normal field points is called inter-grid boundary points. We revise these points by interpolating the solution from the overset grid that created the hole. Values of the interpolation coefficients needed for this revision are automatically provided by a separate algorithm.

3. Computational Grids

Zonal multi-block grids were generated for computations of jet interaction flow fields. These structured multi-block grids have one-to-one overlaps at the zonal boundaries and are H-type grids. The H3P78 projectile can be seen in Figure 1. The initial grid used for these computations was a two-zone grid (see Figure 2) consisting of 1.8 million grid points. The Zone 1 grid along the projectile body has 251 longitudinal points, 59 normal points, and 91 circumferential points, with an H-type grid at the nose of the projectile. The base grid, Zone 2, is an H-grid consisting of 50 longitudinal points, 113 normal points, and 91 circumferential points. The minimum spacing at the wall is 6.0E-05 mm (1.0E-06 calibers).

An expanded view of the base region grid is shown in Figure 3. This figure also shows a jet grid overset onto the after-body grid of the projectile. Figure 4 shows a circumferential cross section of the computational grid at the base of the projectile. It clearly shows the elliptical cross section of the body.

For the jet-on cases, each of the multi-block grids was generated separately. For ease of grid generation, the chimera overset gridding technique (described earlier) was used to model the jet. The projectile body grid was generated first. The chimera technique allows the jet to be gridded separately. Two additional grid zones were created to model the jet. The dimensions for each

zone are 21 x 20 x 40 and 10 x 10 x 40, in the longitudinal, circumferential, and normal directions, respectively. These two zones were then added to the projectile grid for the jet-on calculations, adding about 20,000 points to each grid. One of the jet grids is a cylindrical grid that covers the actual jet and extends beyond (see Figure 5). The second one is a rectangular grid placed within the actual jet and overset onto the other grid primarily to avoid the grid singularity along the centerline of the jet. An expanded view of the jet grids projected onto the projectile surface is shown in Figure 5. The jet grids and the body grids are all overset to form the complete mesh system. The chimera procedure results in hole boundaries (not shown here) in the body grid, which are attributable to the jet, and transfers information between the jet grids along these hole boundaries. The outer boundaries of the jet grids also receive information interpolated from the body mesh.

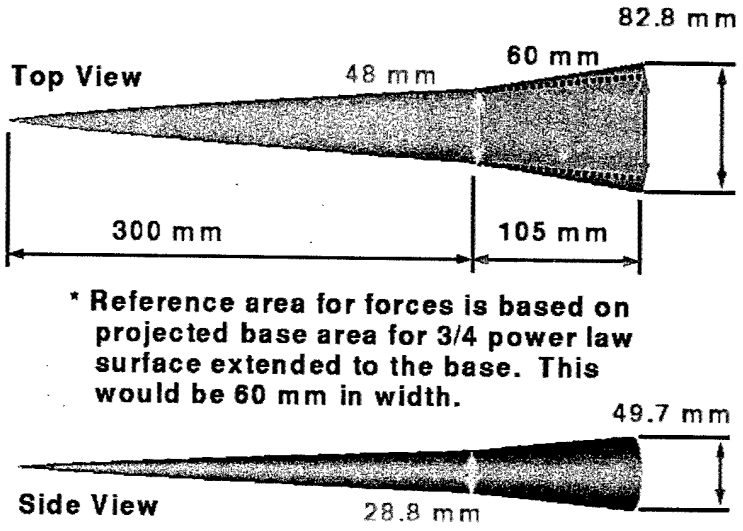

Figure 1. H3P78 projectile.

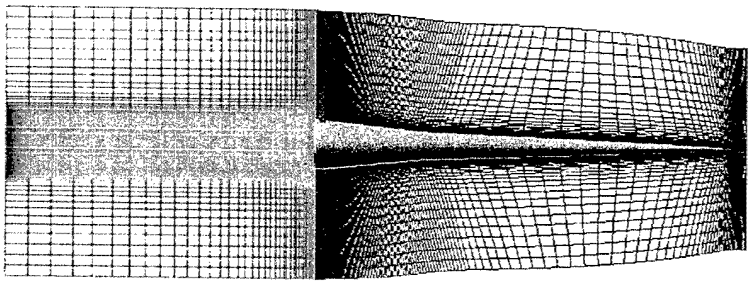

Figure 2. Full grid for viscous computations, jet on.

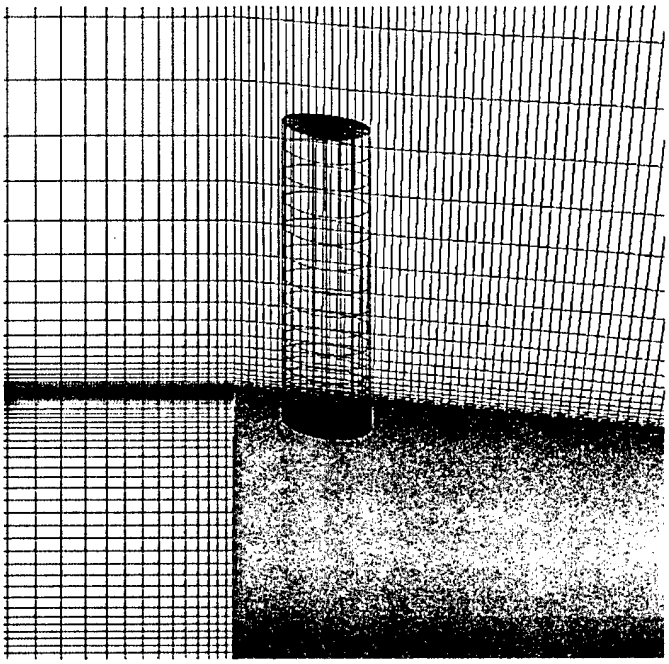

Figure 3. Expanded view of the grid in the base region, jet on.

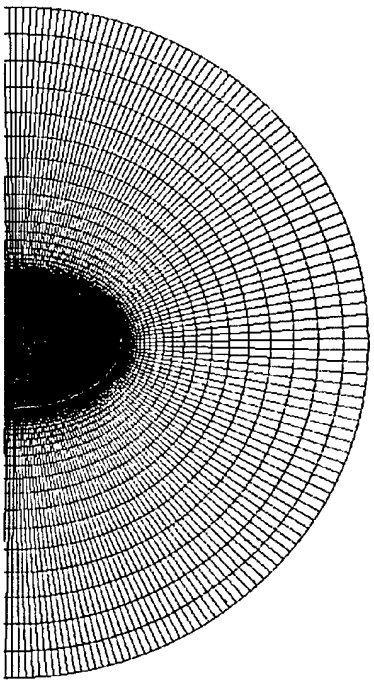

Figure 4. Circumferential cross section of the grid at the base.

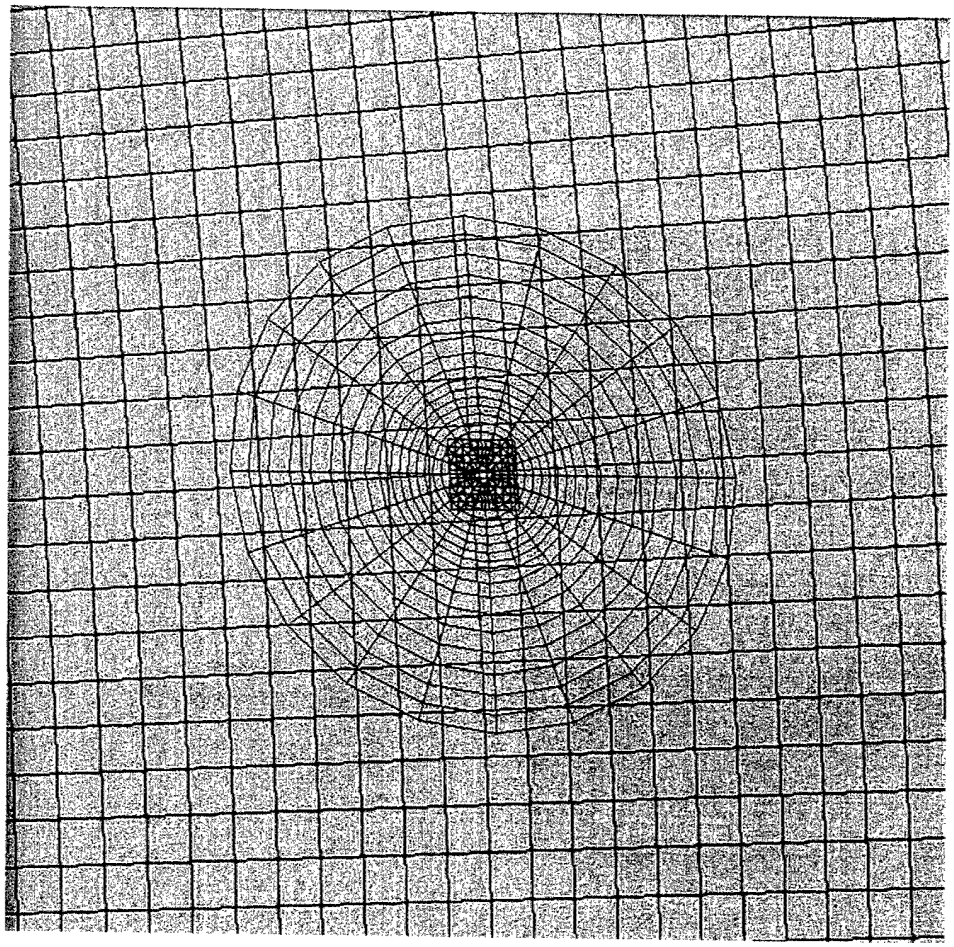

Figure 5. Expanded view of the jet grids projected onto the projectile surface.

A single unstructured grid was generated with 1.8 million grid points for the same problem. In addition, another mesh was generated for the jet-on calculations where the inside of the actual nozzle is modeled (see Figure 6). This is a single zone unstructured grid consisting of about 3.8 million grid points. The grid points are clustered in the near the vicinity of the jet. Also, another grid consisting of a total of 4.6 million points was generated (not shown here) with even more points added in the longitudinal direction in the vicinity of the jet, especially ahead of the jet. The grid blocking used to generate the full grid was left unchanged. Again, the minimum spacing at the wall was selected to yield y+ of about 1.0 in the boundary layer.

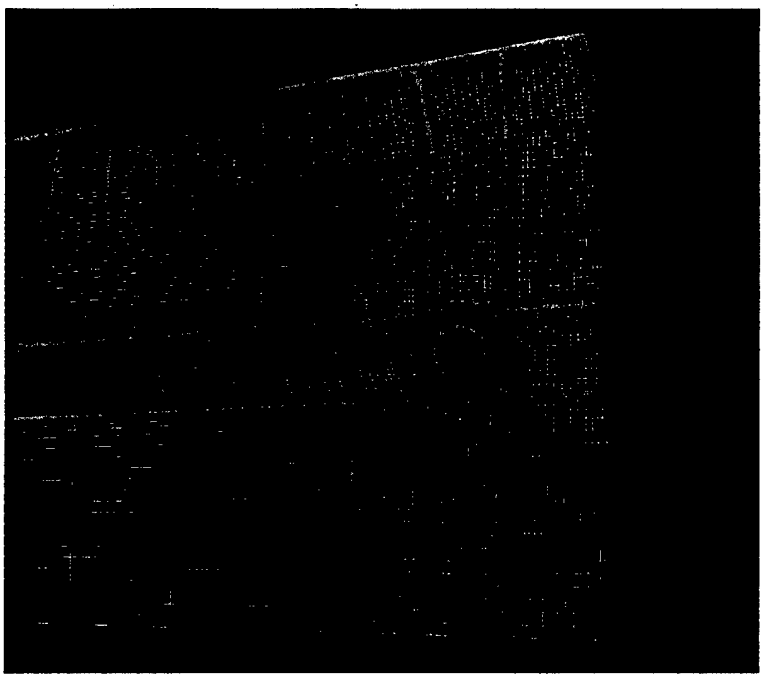

(a)

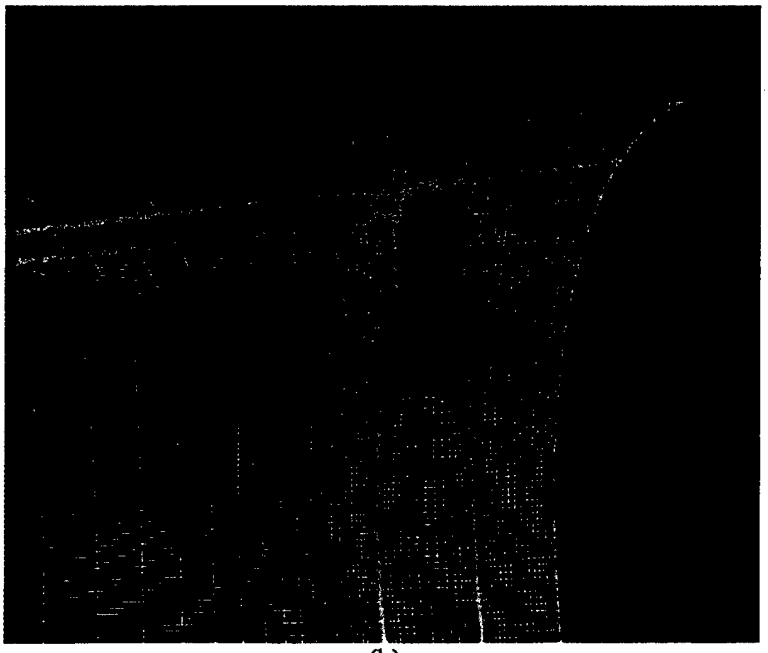

(b)

Figure 6. Expanded view of the grid near the jet with nozzle modeling: (a) top view, (b) side view.

4. Results

Steady state numerical computations made by viscous Navier-Stokes methods were performed to predict the flow field and aerodynamic coefficients on the H3P78 elliptic projectile for jet-on conditions. Three-dimensional numerical computations have been performed for the H3P78 projectile with jet interaction by the CFD++ code at a supersonic Mach number of 4.0 and several angles of attack from 0° to 12°. The real gas version of the CFD++ code was used and the governing equations included air and helium as species. A point-wise two-equation turbulence model was used and integrated all the way to the wall. Because of symmetry, only one of the two helium jets has been modeled in the computations to save computer time. The total pressure, density, and velocity of the jet were set to 21400 Pa, 0.229 kg/m^3, and 872 m/s, respectively. Again, the projectile geometry and a set of experimental wind tunnel data for validation of the computations were supplied by DERA, UK **[12]**. Figure 7 shows the model geometry and the jet locations.

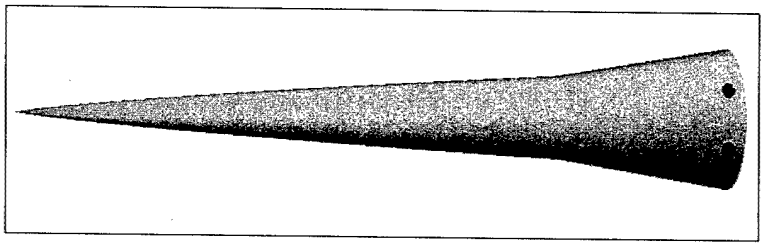

Figure 7. H3P78 projectile showing the jet locations.

A longitudinal cut at the jet centerline was selected and used to show the concentration of helium in that plane containing the jet centerline (see Figure 8) for different jet pressures. Here, black represents zero helium concentration (100% air), and yellow represents high helium concentration. At the jet exit, the helium concentration is 1.0. This figure clearly shows the helium jet interacting with the free-stream flow, the mixing of the two species, and the extent to which it is transferred by convection downstream into the wake region. The size of this interaction region increases with increasing angles of attack. Also, the jet is seen to negotiate more with the lee side free-stream flow at higher angles of attack, resulting in steeper jet angle. This figure also shows the computed surface pressure contours for the different angle-of-attack cases.

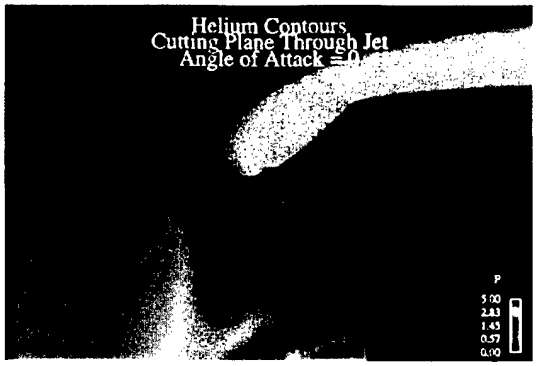

(a)

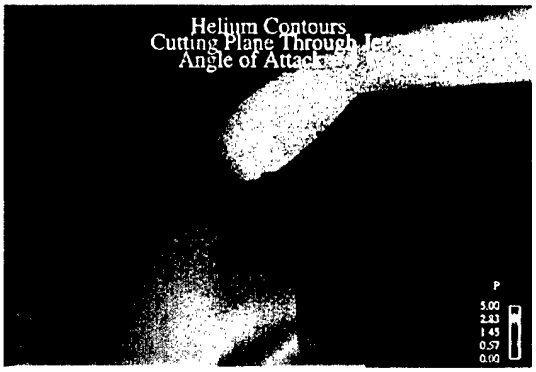

(b)

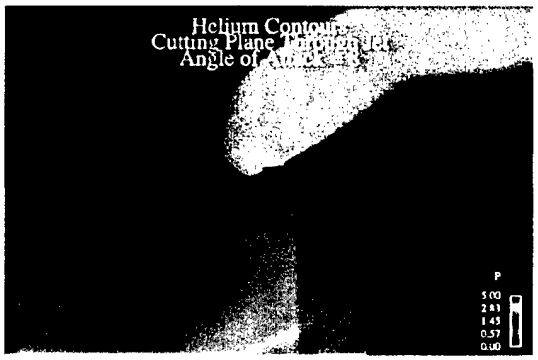

(c)

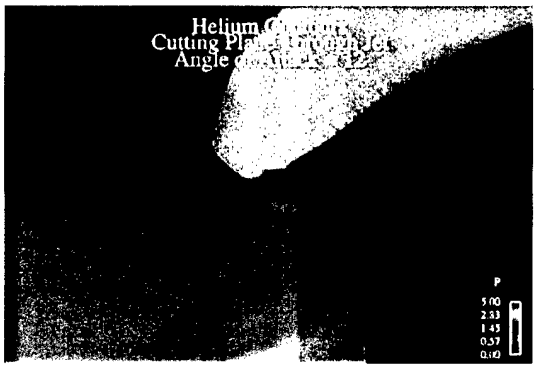

(d)

Figure 8. Computed helium concentration contours near the base region, angle of attack, α = (a) 0°, (b) 4°, (c) 8°, and (d) 12°, M= 4.0.

A circumferential view of the surface pressures on the projectile after-body is shown in Figure 9 for various angles of attack. Here, the low pressure region is indicated in blue, and the high pressure region is indicated in red. The red region on the lee side shows the effect of the jet upstream from and onto the incoming free-stream flow. It clearly shows the strong effect of the jet in all directions for this jet-on case. The surface pressure in front of the jet is increased while the surface pressure downstream from the jet is lower. The upstream influence of the jet is found to increase with increasing angles of attack. The jet affects the pressure as far as the centerline of symmetry, indicating the strong interaction of the two jets in that area. The flow upstream from the jet shock in the flare section is almost unaltered from $\alpha = 0°$ to 4°. At higher angles of attack, one can notice lower pressure on the lee side in that area. It clearly shows the asymmetry (with respect to the jet centerline) in the low pressure region behind the jet at higher angles of attack.

Computed surface pressures have been obtained along the centerline of symmetry and along the centerline of the jet itself. These surface pressures are used to study the effect of the aerodynamic interference resulting from the jet interaction with the free-stream flow. Computed surface pressures have been compared with available experimental data. Figure 10 shows the 3-mm jet holes and the experimental measurement points for surface pressures. Figure 11 shows the comparison of the computed surface pressures with the data measured along the centerline of symmetry for various angle-of-attack cases. The computed results here are shown as lines, and the data are shown as symbols. Both CFD and the data show a pressure rise; however, the numerical predictions indicate a somewhat stronger jet-to-jet interaction than is indicated by the data at lower angles of attack ($\alpha = 0°$ and 4°). At higher angles of attack, the extent of this interaction is decreased, and the computed results are in good agreement with the data. The pressure rise is much less pronounced with increasing angles of attack ($\alpha = 8°$ and 12°). The computed results presented here used the unstructured single mesh (see Figure 6). A finer mesh with more grid points clustered in front of the jet was also used in the computations. The computed results were found to be very similar, with no significant changes in the flow field. It is believed that the discrepancy at lower angles of attack is not attributable to the number of mesh points used in the computations.

A comparison of the computed surface pressures along the centerline of the jet for various angle-of-attack cases is shown in Figure 12. Again, computed results have been compared with the available data. CFD results here at all angles of attack from $\alpha = 0°$ to 12° agree very well with the experimental data. Both CFD and the data clearly show the expected pressure rise ahead of the jet. The extent of upstream influence ahead of the jet is seen to increase with the increase in angle of attack. Also, this figure shows the lower pressures downstream from the jet (pressure less than the free-stream static pressure). This level of lower pressure downstream from the jet also is again very similar to what was measured in the experiment. Overall, the computed flow field around the projectile and the jet showed similar characteristics as those observed in the experiment.

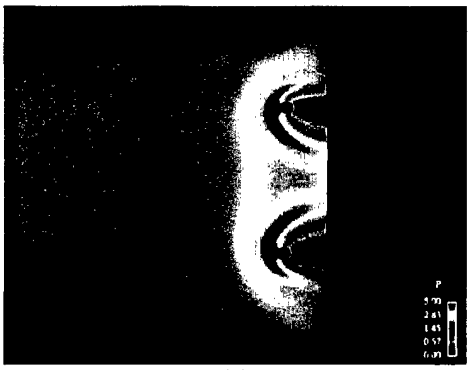

(a)

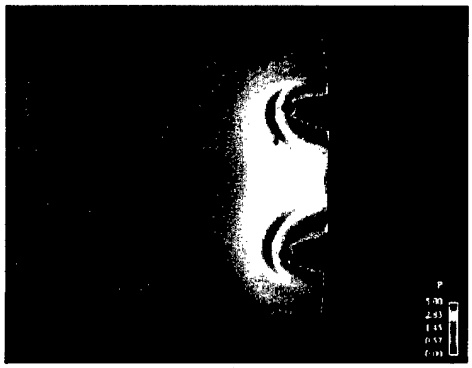

(b)

(c)

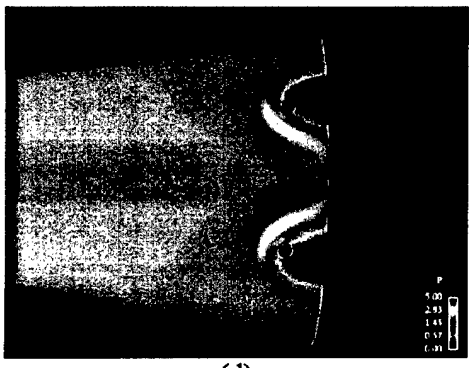

(d)

Figure 9. Computed surface pressure contours, jet on, angle of attack, α = (a) 0°, (b) 4°, (c) 8°, and (d) 12°, M = 4.0.

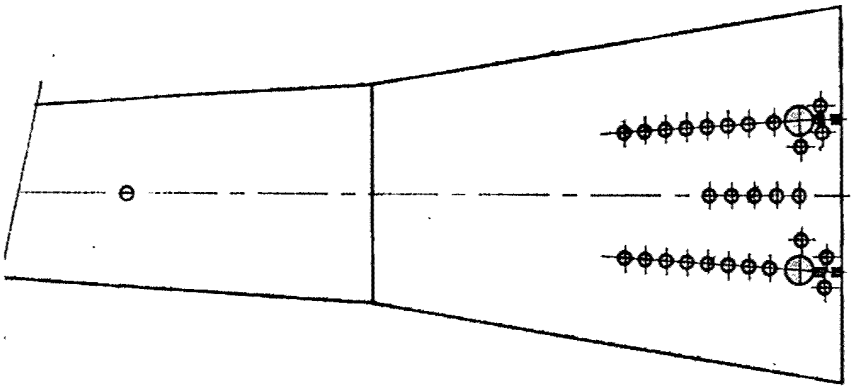

Figure 10. Experimental surface pressure measurement points, M = 4.0.

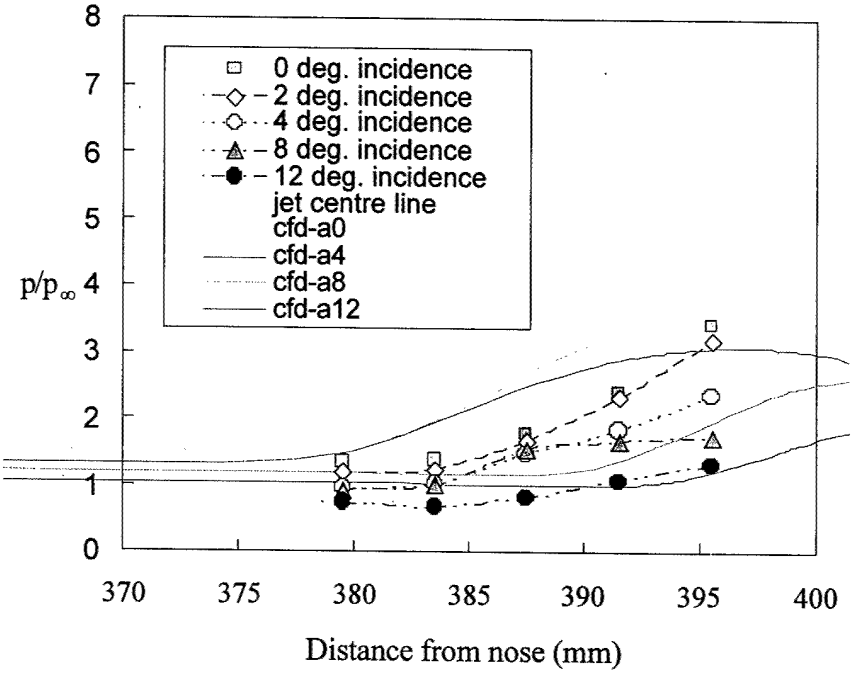

Figure 11. Surface pressure comparison along the centerline of symmetry, M = 4.0.

Computed aerodynamic forces and moments were determined from the flow field results and are shown in Figures 13 and 14. Figure 13 shows the normal force coefficient as a function of angle of attack. Both CFD and the experiment show the normal force coefficient to increase with increasing angle of attack. In general, the CFD results are in agreement with the measured data. CFD results obtained by the chimera multi-block grids seem to match the data very well at low angles of attack; however, there is a small discrepancy in the comparison at high angles of attack. The reverse is true with the CFD results obtained with a single grid with and without nozzle modeling. Modeling the nozzle and computing the nozzle exhaust flow did not seem to change the results from the solution obtained without the nozzle modeled. Figure 14 shows the pitching moment coefficient as a function of angle of attack. Here, the pitching moment coefficient is

referenced to the nose of the projectile. Both CFD and the experiment show the pitching moment to decrease with increasing angle of attack. There is a small discrepancy in the comparison except at low angles of attack, where the chimera solution matches fairly well with the data. Again, the single grid solutions with and without the modeling of the nozzle were essentially the same.

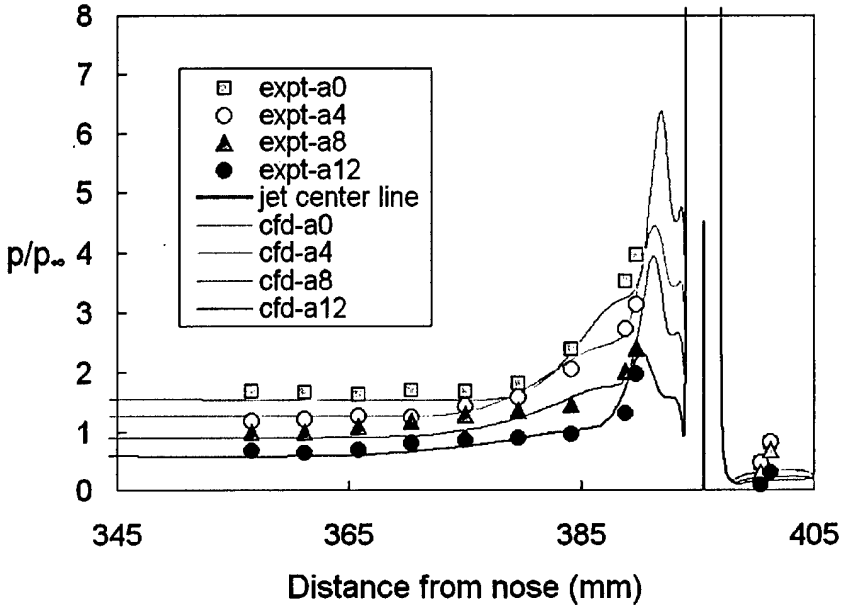

Figure 12. Surface pressure comparison along the centerline of jet, M = 4.0.

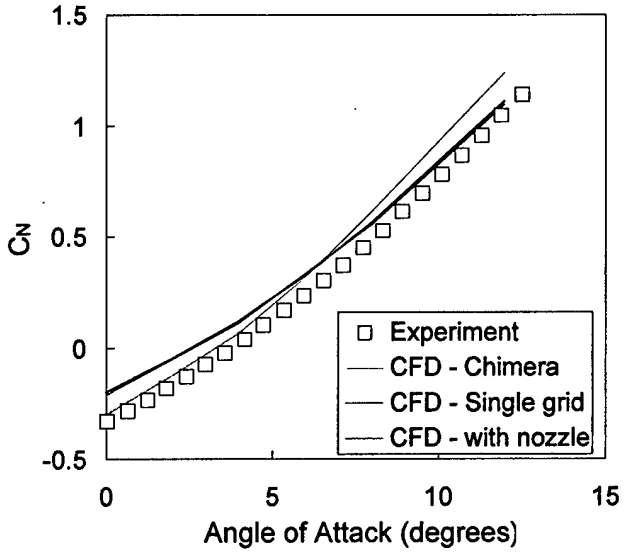

Figure 13. Normal force coefficient, M = 4.0.

Figure 15 shows the amplification factor as a function of angle of attack. The amplification factor is defined as the ratio of the sum of the jet force and the jet interaction force to the jet force alone. As shown in Figure 15, this factor is almost constant in the chimera solution. The

experimental data show a small increase in the amplification factor with increasing angle of attack. This trend can also be clearly observed in the computed results obtained with the single grid CFD with and without nozzle modeling. The nozzle modeling shows a small improvement in the comparison of computed results with the data.

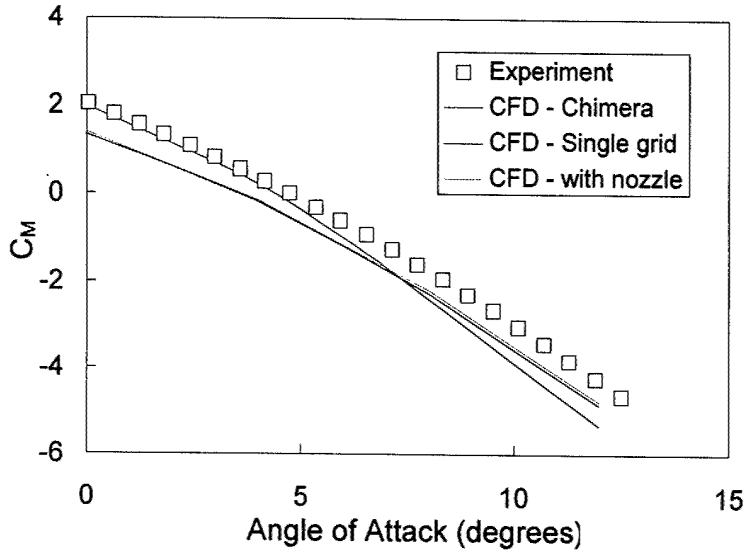

Figure 14. Pitching moment coefficient, M = 4.0.

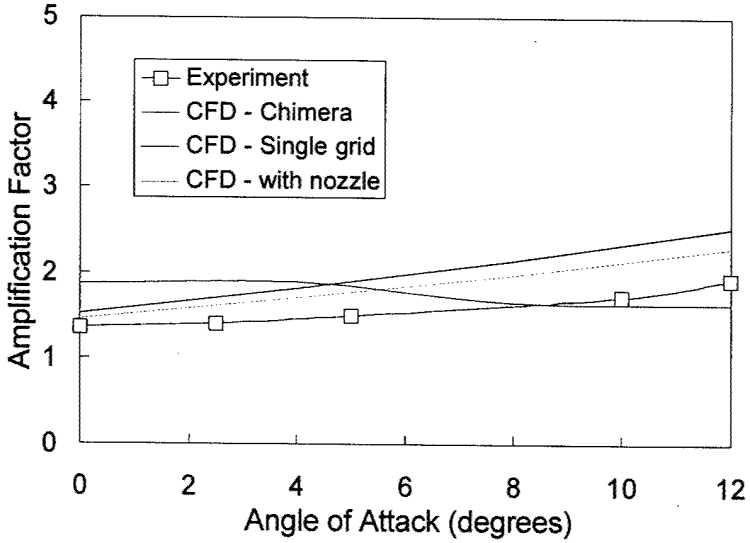

Figure 15. Amplification factor, M = 4.0.

5. Concluding Remarks

CFD approaches were used to compute the supersonic flow fields and aerodynamic forces and moments on elliptic projectiles with jet interaction. Steady state numerical results have been obtained at a supersonic Mach number, Mach = 4.0, and several angles of attack from 0° to 12° for the jet-on conditions by an unstructured Navier-Stokes flow solver. The jet-on cases simulated the interaction of a helium jet with a free-stream M = 4.0 flow. In general, very good agreement of the computed aerodynamic coefficients with the experimental data was achieved at all angles of attack investigated for jet-on conditions. CFD results for the jet-on cases showed the qualitative features and strong flow interaction between the jet and the free-stream flow similar to those observed in the experiment. Computed surface pressures along the jet centerline compared much better than those along the line of symmetry. Computed normal force and pitching moment coefficient matched fairly well with the experimental data. The results showed the predictive capabilities of CFD techniques for supersonic flow over elliptic projectiles with jet interaction.

6. References

1. Sahu, J., Heavey, K.R., Ferry, E.N. Computational Fluid Dynamics for Multiple Projectile Configurations. *Proceedings of the 3rd Overset Composite Grid and Solution Technology Symposium*, Los Alamos, NM, October 1996.

2. Sahu, J., Heavey, K.R., Nietubicz, C.J. Time-Dependent Navier-Stokes Computations for Submunitions in Relative Motion. *Proceedings of the 6th International Symposium on Computational Fluid Dynamics*, Lake Tahoe, NV, September 1995.

3. Sahu, J., Heavey, K.R., Nietubicz, C.J. Computational Modeling of SADARM Submunition Separation. *Journal of Computer Modeling and Simulation in Engineering*, **July 1997**, *2*, 267-283.

4. Sahu, J., Heavey, K.R., Ferry, E.N. Computational Modeling of Multibody Aerodynamic Interference. *Journal of Advances in Engineering Software* **Apr-Jul 1998**, Elsevier Sciences, *29* No. 3-6, 383-388.

5. Orchard, D., Fournier, E., Dupuis, A., Edwards, J. Wind Tunnel Tests on the H3P78, Power Law, Elliptic Section Flared Projectile from Mach 2.5 to 4 inch, *American Institute of Aeronautics and Astronautics (AIAA)* **August 2001** Paper No. 2001-4321, Montreal, Canada.

6. Fournier, E., Orchard, D. *Testing of a Novel Maneuvering Projectile in the DREV Trisonic Wind Tunnel*, Technical Memorandum Report DREV TM-2000-108, Defence Research Establishment, Valcartier, Canada, July 2000.

7. Edge, H.L., Clarke, J. *Graphical User Interface for ZEUS*, ARL-TR-1093, U.S. Army Research Laboratory: Aberdeen Proving Ground, MD, June 1996.

8. Sahu, J., Heavey, K.R., Edge, H.L. Numerical Computations of Supersonic and Hypersonic Flow over Elliptical Projectiles, *AIAA* **August 2001** Paper No. 2001-4320, Montreal, Canada.

9. Edge, H.L., Sahu, J., Sturek, W.B., Pressl, D.M., Heavey, K.R., Weinacht, P., Zoltani, C.K., Nietubicz, C.J., Clarke, J., Behr, M., Collins, P. *Common High Performance Computing Software Support Initiative (CHSSI) Computational Fluid Dynamics (CFD)-6 Project Final Report: ARL Block-Structured Gridding Zonal Navier-Stokes (ZNSFLOW) Solver Software*. ARL-TR-2084, U.S. Army Research Laboratory: Aberdeen Proving Ground, MD, February 2000.

10. Peroomian, O., Chakravarthy S., Goldberg, U.C. A "Grid-Transparent" Methodology for CFD, *AIAA* **1997,** Paper 97-07245.

11. Peroomian, O., Chakravarthy S., Palaniswamy, S., Goldberg, U.C. Convergence Acceleration for Unified Grid Formulation using Preconditioned Implicit Relaxation, *AIAA* **1998,** Paper 98-0116.

12. Orchard, D., Fournier, E., Dupuis, A., Edwards, J. Wind Tunnel Tests on the H3P78, Power Law, Elliptic Section Flared Projectile with Jet Interaction, *AIAA* **August 2001,** Paper No. 2001-4322, Montreal, Canada.

13. Steger, J.L., Dougherty, F.C., Benek, J.A. A Chimera Grid Scheme, *Advances in Grid Generation*, edited by K. N. Ghia and U. Ghia, ASME FED-5, June 1983.

14. Benek, J.A., Donegan, T.L., Suhs, N.E. Extended Chimera Grid Embedding Scheme With Application to Viscous Flows. *AIAA* **1987**, Paper No. 87-1126-CP.

15. Meakin, R., Wissink, A. Unsteady Aerodynamic Simulation of Static and Moving Bodies Using Scalable Computers, AIAA-99-3302-CP, *14th AIAA Computational Fluid Dynamics Conference*, Norfolk, VA, June 1999.

16. Goldberg, U.C., Peroomian, O., Chakravarthy S. A Wall-Distance-Free K-E Model With Enhanced Near-Wall Treatment, *ASME Journal of Fluids Engineering* **1998**, *120*, 457-462.